



OPEN

Non-Fourier energy transmission in power-law hybrid nanofluid flow over a moving sheet

Awatif Alhawaity¹, Muhammad Bilal², Haneen Hamam³, M. M. Alqarni⁴, Kanit Mukdasai⁵✉ & Aatif Ali⁶

Ethylene glycol is commonly used as a cooling agent in the engine, therefore the study associated with EG has great importance in engineering and mechanical fields. The hybrid nanofluid has been synthesized by adding copper and graphene nanoparticles into the Ethylene glycol, which obeys the power-law rheological model and exhibits shear rate-dependent viscosity. As a result of these features, the power-law model is utilized in conjunction with thermophysical characteristics and basic rules of heat transport in the fluid to simulate the physical situations under consideration. The Darcy Forchhemier hybrid nanofluid flow has been studied under the influence of heat source and magnetic field over a two-dimensionally stretchable moving permeable surface. The phenomena are characterized as a nonlinear system of PDEs. Using resemblance replacement, the modeled equations are simplified to a nondimensional set of ODEs. The Parametric Continuation Method has been used to simulate the resulting sets of nonlinear differential equations. Figures and tables depict the effects of physical constraints on energy, velocity and concentration profiles. It has been noted that the dispersion of copper and graphene nanoparticulate to the base fluid ethylene glycol significantly improves velocity and heat conduction rate over a stretching surface.

Industrial and natural fluids detract from Newton's viscosity law because their viscosity does not correlate with deformation rate. These fluids are recognized as non-Newtonian fluids (NNF). They are further subdivided into numerous classes. There are some notorious classes of NNF, whose shear rate is not independent of flow direction. Shear rate-dependent viscosity fluids are subdivided further Herschel–Bulkley, Casson fluids, Bingham fluids, Carreau–Yasuda fluid, Carreau fluids and power-law fluid^{1–6}. Minakov et al.⁷ described the findings of a practical assessment of the nanofluids (NF) flow incorporating nano particulates of various metals and oxides. Al-Mubaddel et al.⁸ has utilized the rheological model to predict the energy and mass transfer via hybrid NF fluid subjected to a magnetic field. The findings revealed that the transport of species in a power-law fluid is influenced by the opposite trends of chemical reactions. Using a power law fluid model, Cheng⁹ studied the energy and mass transmission. A porous, parallel plate microreactor with NN working fluid was inspected by Javidi et al.¹⁰ with the transfer of heat and mass, as well as thermodynamic irreversibility. The results show that Microreactor thermodynamic irreversibility is shown to be affected by wall thickness and thermal variance. Chavaraddi et al.¹¹ examined the thermal properties of a passive conducting fluid in a bounded domain subjected to external effects. The results exposed that a power-law fluid stabilize the system while an electric field or magnetic field destabilizes the interface. Alsallami et al.¹² develop an Maxwell nanofluid flow with arrhenius activation energy over a rotating disk. The dynamics of a bubble confined within an elastic solid in a non-Newtonian power-law fluid are investigated by Arefmanesh et al.¹³. The numerical examination of 2D non-Newtonian power-law fluids through a circular cylinder is presented by Bilal et al.¹⁴. The conclusions show that the system's frequency and apparent viscosity have a significant impact on the VIV of the cylinder's properties. Elattar et al.¹⁵ studied the power-law fluid flows past over a porous slender stretching surface. Some recent contributions have been made by many researchers towards power-law fluid flow through porous enlarging surface^{16–19}.

Heat and mass transfer are utilized in a wide range of industries, including heating and air conditioning, energy systems, cars, steam-electric power production, disease detection and electronic device cooling^{20–24}.

¹Department of Mathematics, College of Science and Arts at Alkamil, University of Jeddah, Jeddah, Saudi Arabia. ²Department of Mathematics, City University of Science and Information Technology, Peshawar 25000, Pakistan. ³Mathematics Department, Umm Al-Qura University, Makkah, Saudi Arabia. ⁴Department of Mathematics, College of Sciences, King Khalid University, Abha 61413, Saudi Arabia. ⁵Department of Mathematics, Faculty of Science, Khon Kaen University, Khon Kaen 40002, Thailand. ⁶Department of Mathematics, Abdul Wali Khan University Mardan, Khyber Pakhtunkhwa 23200, Pakistan. ✉email: kanit@kku.ac.th

Ordinary fluid, on the other hand, is unable to meet this requirement of heat transition. As a result, the incorporation of NPs in the base fluid is very suggestive. Nanofluids have gotten a lot of attention in the previous decade, especially in heat transfer enhancement and renewable energy. Nanofluids are used in ocean power plants, thermodynamics, solar collectors, hydropower rotors, geothermal heat exchangers and wind turbines^{25–30}. Jia et al.³¹ described a realistic approach for synthesizing cell membrane (CM)-coated iron oxide nanoclusters as a nanocarrier for anticancer medicine. Iron oxide nanoparticles were used by Schwaminger et al.³² to design novel flotation process approaches that took use of their particular features. An alkaline coprecipitation procedure was used to create magnetic nanoparticles with a basic crystal structure of 9 nm, which were subsequently coated with sulfate. A study conducted by Bilal et al.³³ considered the impacts of Hall current on the flow of carbon nanotubes and iron ferrite hybrid nanoliquids along the surface of a spinning disc.

The C–C bond makes CNTs in base fluid more effective than other nanocomposite forms. The desired outcome can be obtained by covalent or non-covalent manipulation of CNT nanofluid^{34–36}. Ferrofluid flow across an endless, impermeable disc was analyzed by Tassaddiq et al.³⁷. They found that the combination of CNTs and Fe₂O₃ nanoparticles significantly increases the transfer of energy and mass. CNT + Fe₂O₃/H₂O has a stronger impact on carrier fluid thermophysical parameters than magnetic ferrite nanoparticles. Bilal et al.³⁸ scrutinized the cumulative upshots of electro- and magneto-hydrodynamics on the flow of water-based hybrid nanofluids over two collateral sheets in a two-collateral sheet arrangement. Ullah et al.³⁹ numerically investigated an unstable squeezed flow of a HNF comprising CNTs and CuO, as well as a nanofluid containing CNTs. In an experimental context, Alharbi et al.⁴⁰ calculated the upshot of particle and energy concentration on the dynamic of hybrid nanoliquid. The results show that by increasing the number of nanoparticles, the viscosity increases up to 168 percent. Ullah et al.⁴¹ investigated how a hybrid nanofluid flow on the outside of a revolving disc could improve mass and heat conduction. They observed that hybrid nanofluids are more successful at transporting heat than regular nanofluids^{42–46}. discuss the further uses, synthesis, utilization, and structural characteristics of magnetic nanomaterials and carbon nanotubes.

It has been revealed that fluids with shear rate-dependent viscosity can return to their thermal equilibrium state as a result of the thermal relaxation time features of the fluids^{47,48}. Heat and mass transmission through convective Maxwell nanoliquid across an extending sheet was studied by Sui et al.⁴⁹ using the Cattaneo–Christov (CC) double-diffusion model. The results show that this viscoelastic relaxation framework system predicts relaxation timings transport properties. The CC theory is used by Hafeez et al.⁵⁰ instead of traditional Fourier's and Fick's laws to investigate the energy propagation in the fluid. Manjunatha et al.⁵¹ and Naveen et al.⁵² inspected the energy and mass transportation mechanisms caused by a chemical reaction, thermophoresis effect and Brownian motion in a stream of viscous nanocomposites submitted to a curvy stretched surface. Madhukesh et al.⁵³ considered CC double diffusion models to investigate 3D Prandtl liquid flow. Similar studies related to the proposed model can be found in refs^{54,55}.

The literature revealed that no investigation on the argumentation of energy transmission in a power-law fluid due to the combined dispersion of Cu and Graphene nanoparticles has been found. The motive of the research is to develop a computational model using copper and Graphene nanoparticles in the carrier fluid ethylene glycol, to magnify the energy communication rate and boost the competence and ability of thermal energy transference for a variety of biological and commercial purposes. Furthermore, the PCM procedure has been used to tackle the modeled equations of the proposed model.

Mathematical formulation

We considered a 2D HNF flow over a stretchable moving surface with fixed temperature T_w with velocity $V_w = ax\hat{i} + by\hat{j}$, the sheet surface is moving. The non-Newtonian hybrid nanofluid fluid, flow over the surface, obeys the power-law rheological model. Figure 1 revealed the physical mechanism of the fluid flow over a moving permeable surface. The energy transport mechanism is supposed to be augmented with the dispersion of nanoparticles Copper and Graphene. The wall of sheet is moving with 2D velocity, but as a result the heat transfer and of fluid flow will be 3D. The basic equation, which regulates the fluid flow and energy transport mechanism are as follow^{27,56,57}:

Continuity equation

$$\frac{\partial u}{\partial x} + \frac{\partial v}{\partial y} + \frac{\partial w}{\partial z} = 0, \quad (1)$$

Momentum equation along x -axis

$$u \frac{\partial u}{\partial x} + v \frac{\partial u}{\partial y} + w \frac{\partial u}{\partial z} = \frac{k_1}{\rho_{hnf}} \frac{\partial}{\partial z} \left(\left| \frac{\partial u}{\partial z} \right|^{n-1} \frac{\partial u}{\partial z} \right) - \left(\frac{\sigma_{hnf} B_0^2}{\rho_{hnf}} (u - v) \right) - \frac{\nu_{hnf}}{K^*} u - \frac{1}{\rho_{hnf}} F u^2, \quad (2)$$

Momentum equation along y -axis

$$u \frac{\partial v}{\partial x} + v \frac{\partial v}{\partial y} + w \frac{\partial v}{\partial z} = \frac{k_1}{\rho_{hnf}} \frac{\partial}{\partial z} \left(\left| \frac{\partial v}{\partial z} \right|^{n-1} \frac{\partial v}{\partial z} \right) - \left(\frac{\sigma_{hnf} B_0^2}{\rho_{hnf}} (u + v) \right) - \frac{\nu_{hnf}}{K^*} v - \frac{1}{\rho_{hnf}} F v^2, \quad (3)$$

Energy equation

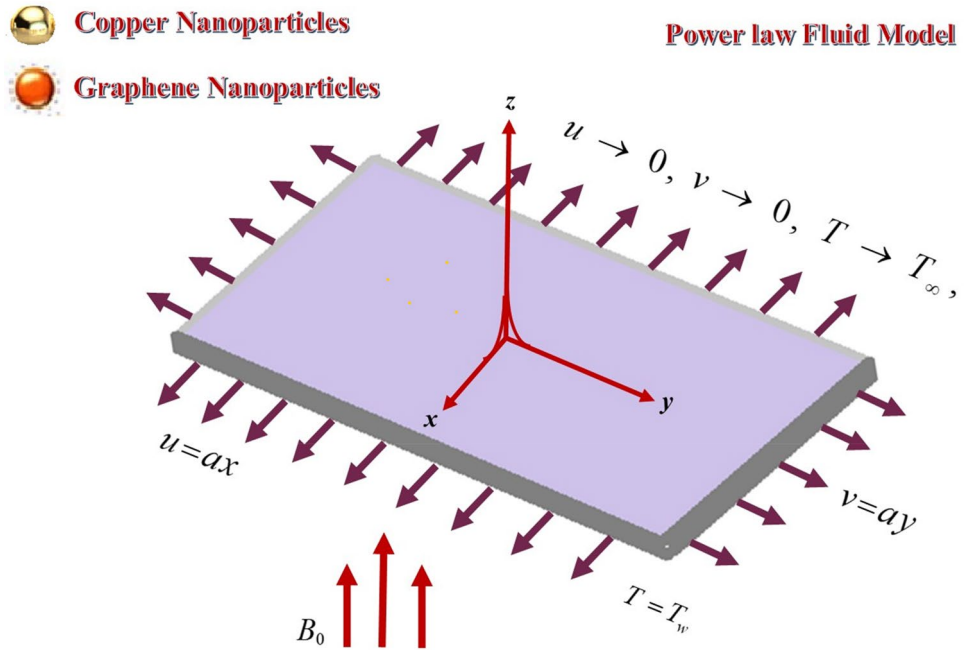


Figure 1. Hybrid nanofluid flow over a moving permeable surface.

$$\begin{aligned}
 & u \frac{\partial T}{\partial x} + v \frac{\partial T}{\partial y} + w \frac{\partial T}{\partial z} + \lambda_1 \left(u^2 \frac{\partial^2 T}{\partial x^2} + w^2 \frac{\partial^2 T}{\partial z^2} + v^2 \frac{\partial^2 T}{\partial y^2} + 2vw \frac{\partial^2 T}{\partial y \partial z} + 2uv \frac{\partial^2 T}{\partial x \partial y} + 2uw \frac{\partial^2 T}{\partial x \partial z} \right. \\
 & \left. + \left(u \frac{\partial u}{\partial x} + w \frac{\partial u}{\partial z} + v \frac{\partial u}{\partial y} \right) \frac{\partial T}{\partial x} - \frac{Q_0}{(\rho C_p)_{hnf}} \left(u \frac{\partial T}{\partial x} + w \frac{\partial T}{\partial z} + v \frac{\partial T}{\partial y} \right) \right) \\
 & \left. + \left(u \frac{\partial v}{\partial x} + w \frac{\partial v}{\partial z} + v \frac{\partial v}{\partial y} \right) \frac{\partial T}{\partial y} + \left(u \frac{\partial w}{\partial x} + w \frac{\partial w}{\partial z} + v \frac{\partial w}{\partial y} \right) \frac{\partial T}{\partial z} \right) \\
 & = \frac{k_{hnf}}{(\rho C_p)_{hnf}} \frac{\partial^2 T}{\partial y^2} + \frac{Q_0(T - T_\infty)}{(\rho C_p)_{hnf}}.
 \end{aligned} \tag{4}$$

$$\left. \begin{aligned}
 & u = ax = U_w, \quad v = by = V_w, \quad T - T_w = 0, \quad w = 0 \quad \text{as } z = 0, \\
 & u \rightarrow 0, \quad v \rightarrow 0, \quad T \rightarrow T_\infty \quad \text{as } z \rightarrow \infty.
 \end{aligned} \right\} \tag{5}$$

here U_w and V_w represents that the surface is stretching along both x -axis and y -axis directions.

Similarity transformation

The similarity variables are defined as⁵⁹:

$$\begin{aligned}
 & u = axf'(\eta), \quad w = -a \left(\frac{ba^{n-2}}{\rho_f} \right)^{\frac{1}{n+1}} \left(\frac{2n}{n+1} f(\eta) + \frac{1-n}{1+n} \eta f'(\eta) + g(\eta) \right) x^{\frac{n-1}{n+1}}, \quad v = ybg'(\eta), \\
 & \theta(\eta) = \frac{T - T_\infty}{T_w - T_\infty}, \quad \eta = z \left(\frac{ba^{n-2}}{\rho_f} \right)^{\frac{1}{n+1}} x^{\frac{1-n}{1+n}}
 \end{aligned} \tag{6}$$

Incorporating Eq. (6) into Eqs. (1-4), we get:

$$\begin{aligned}
 & \left(|f''|^{n-1} f' \right)' - (1 - \varphi_2) \left((1 - \varphi_1) + \varphi_1 \frac{\rho_{s1}}{\rho_f} \right) + \varphi_2 \frac{\rho_{s2}}{\rho_f} \left[Frf'^2 + \left(\frac{2n}{n+1} f + g \right) f'' \right] \\
 & - (1 - \varphi_1)^{2.5} (1 - \varphi_2)^{2.5} \frac{\sigma_{hnf}}{\sigma_f} M^2 (\lambda f' - g') = 0,
 \end{aligned} \tag{7}$$

$$\begin{aligned} & \left(|f''|^{n-1} g'' \right)' - (1 - \varphi_2) \left[(1 - \varphi_1) + \varphi_1 \frac{\rho_{s1}}{\rho_f} \right] + \varphi_2 \frac{\rho_{s2}}{\rho_f} \left[Fr g'^2 + \left(\frac{2n}{n+1} f + g \right) g'' \right] \\ & - (1 - \varphi_1)^{2.5} (1 - \varphi_2)^{2.5} \frac{\sigma_{hmf}}{\sigma_f} M^2 (2\lambda g') = 0, \end{aligned} \tag{8}$$

$$\begin{aligned} & \theta'' + \frac{k_f(\rho C_p)_{hmf}}{k_{hmf}(\rho C_p)_f} \left[Pr \left(\frac{2n}{n+1} \right) f \theta' + Pr g \theta \right] + \frac{k_f}{k_{hmf}} h_s \left(\frac{2n}{n+1} \right) Pr \theta \\ & - \frac{k_f(\rho C_p)_{hmf}}{k_{hmf}(\rho C_p)_f} Pr \lambda_E \left\{ \left(\frac{2n}{n+1} f + g \right) \left(\frac{2n}{n+1} f' + g' \right) \theta' \left(\frac{2n}{n+1} f + g \right)^2 \theta'' + h_s Pr \left(\frac{2n}{n+1} f + g \right) \theta' \right\} = 0. \end{aligned} \tag{9}$$

Incorporating \wp_1, \wp_2, \wp_3 in Eqs. (7–9) for simplification purpose, where \wp_1, \wp_2, \wp_3 are defined as:

$$\wp_1 = (1 - \varphi_2) \left((1 - \varphi_1) + \varphi_1 \frac{\rho_{s1}}{\rho_f} \right) + \varphi_2 \frac{\rho_{s2}}{\rho_f}, \quad \wp_2 = (1 - \varphi_1)^{2.5} (1 - \varphi_2)^{2.5} \frac{\sigma_{hmf}}{\sigma_f}, \quad \wp_3 = \frac{k_f(\rho C_p)_{hmf}}{k_{hmf}(\rho C_p)_f}.$$

we get

$$\left(|f''|^{n-1} f'' \right)' - \wp_1 \left(Fr f'^2 + \left(\frac{2n}{n+1} f + g \right) f'' \right) - \wp_2 M^2 (\lambda f' - g') = 0, \tag{10}$$

$$\left(|f''|^{n-1} g'' \right)' - \wp_1 \left(Fr g'^2 + \left(\frac{2n}{n+1} f + g \right) g'' \right) - \wp_2 M^2 (2\lambda g') = 0, \tag{11}$$

$$\left. \begin{aligned} & \theta'' + \wp_3 \left(Pr \left(\frac{2n}{n+1} \right) f \theta' + Pr g \theta \right) + \frac{k_f}{k_{hmf}} h_s \left(\frac{2n}{n+1} \right) Pr \theta - \wp_3 Pr \lambda_E \\ & \left\{ \left(\frac{2n}{n+1} f + g \right) \left(\frac{2n}{n+1} f' + g' \right) \theta' \left(\frac{2n}{n+1} f + g \right)^2 \theta'' + h_s Pr \left(\frac{2n}{n+1} f + g \right) \theta' \right\} = 0. \end{aligned} \right\} \tag{12}$$

The boundary conditions are given below:

$$\left. \begin{aligned} & f(0) = 0, \quad f'(0) = g'(0) = 1, \quad g(0) = 0, \quad \theta(0) = 1 \\ & f(\infty) = 0, \quad g(\infty) = 0, \quad \theta(\infty) = 0. \end{aligned} \right\} \tag{13}$$

here $M^2 = \frac{2\sigma_f B_0^2}{a\rho_f}$ is the Hartmann number, $h_s = \frac{Q}{a(C_p)_f \rho_f}$ is the heat generation term, $\lambda_E = \frac{a\lambda_1}{x}$ is the thermal relaxation constraint, $Re = \frac{x^n (U_w)^{2-n} \rho_f}{k_f}$ is the Reynolds number, $Pr = \frac{(C_p)\rho_f a x^2 Re^{\frac{2}{n-1}}}{k_f}$ is the Prandtl number and $Fr = \frac{x C_b}{\sqrt{K^*}}$ is the Darcy Forchhemier number. where, s_1 and s_2 represent the Copper and Graphene nanoparticles respectively.

The skin friction expressed as:

$$\frac{1}{2} C_f (Re)^{\frac{1}{n+1}} = \frac{|f''(0)|^n}{(1 - \varphi_1)^{2.5} (1 - \varphi_2)^{2.5}}, \quad \frac{1}{2} C_g (Re)^{\frac{1}{n+1}} = \frac{|f''(0)|^{n-1} g''(0)}{(1 - \varphi_1)^{2.5} (1 - \varphi_2)^{2.5}}. \tag{14}$$

The heat transfer rate can be stated as:

$$Nu = \frac{xq_w}{K_f(T_w - T_\infty)}, \quad q_w = -k_{hmf} \frac{\partial T}{\partial z} \Big|_{\text{at wall}}, \quad (Re)^{0.5} Nu = \frac{k_{hmf}}{k_f} \theta'(0). \tag{15}$$

Numerical solution

The main steps, while dealing with PCM method are^{60–63}:

Step 1 Converting the system of BVP to the ODEs

$$\left. \begin{aligned} & \tilde{h}_1(\eta) = f(\eta), \quad \tilde{h}_2(\eta) = f'(\eta), \quad \tilde{h}_3(\eta) = g(\eta), \\ & \tilde{h}_4(\eta) = g'(\eta), \quad \tilde{h}_5(\eta) = \theta(\eta), \quad \tilde{h}_6(\eta) = \theta'(\eta). \end{aligned} \right\} \tag{16}$$

By putting Eq. (16) in Eq. (10–13), we get:

$$\left(|\tilde{h}'_2|^{n-1} \tilde{h}'_2 \right)' - \wp_1 \left(Fr \tilde{h}_2^2 + \left(\frac{2n}{n+1} \tilde{h}_1 + \tilde{h}_3 \right) \tilde{h}'_2 \right) - \wp_2 M^2 (\lambda \tilde{h}_2 - \tilde{h}_4) = 0, \tag{17}$$

$$\left(|\hbar'_2|^{n-1}\hbar'_4\right)' - (\wp_1 Fr \hbar_4 + 2\lambda\wp_2 M^2)\hbar_4 - \wp_1\left(\frac{2n}{n+1}\hbar_1 + \hbar_3\right)\hbar'_4 = 0, \tag{18}$$

$$\begin{aligned} \hbar'_6 - \wp_3 Pr \lambda_E \left\{ \begin{aligned} &\wp_3 Pr \left(\frac{2n}{n+1}\right)\hbar_1 + \left(\hbar_1 \frac{2n}{n+1} + \hbar_3\right)\left(\frac{2n}{n+1}\hbar_2 + \hbar_4\right) \\ &\left(\frac{2n}{n+1}\hbar_1 + \hbar_3\right)^2 \hbar'_6 + h_s Pr \left(\frac{2n}{n+1}\hbar_1 + \hbar_3\right) \end{aligned} \right\} \hbar_6 \\ + \wp_3 Pr \hbar_5 \hbar_3 + \frac{k_f}{k_{hmf}} h_s \left(\frac{2n}{n+1}\right) Pr \hbar_5 = 0. \end{aligned} \tag{19}$$

the boundary conditions are:

$$\left. \begin{aligned} \hbar_1(0) = \hbar_3(0) = 0, \quad \hbar_2(0) = \hbar_4(0) = 1, \quad \hbar_5(0) = 1 \\ \hbar_1(\infty) = \hbar_3(\infty) = 0, \quad \hbar_5(\infty) = 0. \end{aligned} \right\} \tag{20}$$

Step 2 Introducing the embedding parameter p in Eqs. (17–19):

$$\left(|\hbar'_2|^{n-1}\hbar'_2\right)' - (\wp_1 Fr \hbar_2 + \wp_2 M^2 \lambda)(\hbar_2 - 1)p + \wp_2 M^2 \hbar_4 - \wp_1\left(\hbar_1 \frac{2n}{n+1} + \hbar_3\right)\hbar'_2 = 0, \tag{21}$$

$$\left(|\hbar'_4|^{n-1}\hbar'_4\right)' - (\wp_1 Fr \hbar_4 + 2\lambda\wp_2 M^2)(\hbar_4 - 1)p - \wp_1\left(\frac{2n}{n+1}\hbar_1 + \hbar_3\right)\hbar'_4 = 0, \tag{22}$$

$$\begin{aligned} \hbar'_6 - \wp_3 Pr \lambda_E \left\{ \begin{aligned} &\wp_3 Pr \left(\frac{2n}{n+1}\right)\hbar_1 + \left(\frac{2n}{n+1}\hbar_1 + \hbar_3\right)\left(\frac{2n}{n+1}\hbar_2 + \hbar_4\right) \\ &\left(\frac{2n}{n+1}\hbar_1 + \hbar_3\right)^2 \hbar'_6 + h_s Pr \left(\frac{2n}{n+1}\hbar_1 + \hbar_3\right) \end{aligned} \right\} (\hbar_6 - 1)p + \\ \wp_3 Pr \hbar_5 \hbar_3 + \frac{k_f}{k_{hmf}} h_s \left(\frac{2n}{n+1}\right) Pr \hbar_5 = 0. \end{aligned} \tag{23}$$

Step 3 Differentiating by parameter 'p'

$$V' = \Delta V + R, \tag{24}$$

where Δ is the coefficient matrix.

$$V = \frac{d\hbar_i}{d\tau} \tag{25}$$

where $i = 1, 2, \dots, 11$.

Step 4 Apply the Cauchy Principal

$$V = aU + W, \tag{26}$$

where W and U are the indefinite vector functions.

$$U' = aU, \tag{27}$$

$$W' = \Delta W + R, \tag{28}$$

Using Eq. (26) in Eq. (24), we get

$$(aU + W)' = \Delta(aU + W) + R, \tag{29}$$

Step 5 Solving the Cauchy problems

$$\frac{U^{i+1} - U^i}{\Delta\eta} = \Delta U^{i+1}, \quad \frac{W^{i+1} - W^i}{\Delta\eta} = \Delta W^{i+1}. \tag{30}$$

Finally, we get:

$$U^{i+1} = (I - \Delta\Delta\eta)^{-1}U^i, \quad W^{i+1} = (I - \Delta\Delta\eta)^{-1}(W^i + \Delta\eta R). \tag{31}$$

Results and discussion

This section explains the physical mechanism behind each result, which is shown in the Figures and Table.

Figures 2, 3, 4 and 5 revealed the conduct of velocity contour $f'(\eta)$ versus the variation of nanoparticles volume friction ϕ , Darcy Forchhemier term Fr , magnetic term M and parameter n (for $n = 1$, the fluid behave

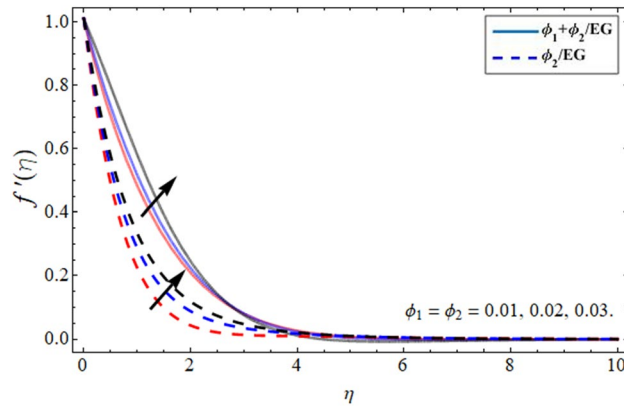


Figure 2. Velocity $f'(\eta)$ outlines versus the effect of nanoparticles volume fraction ϕ .

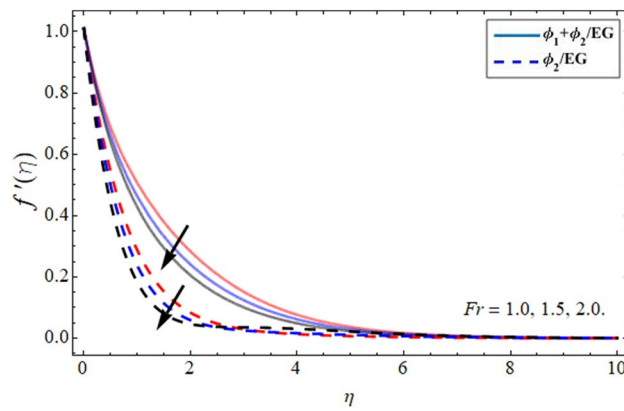


Figure 3. Velocity $f'(\eta)$ outlines versus the effect of Darcy Forchhemier term Fr .

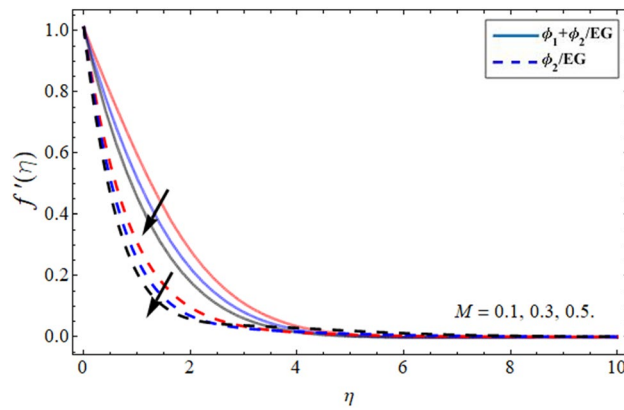


Figure 4. Velocity $f'(\eta)$ outlines versus the effect of magnetic term M .

as Newtonian, while at $n > 1$, the shear thickening phenomena occur) respectively. Figure 2 reported that the axial velocity outline boosts with the addition of hybrid NPs in EG. Physically, the specific heat capacity of ethylene glycol is greater than copper and graphene NPs, so the addition of nanoparticles declines its thermal absorbing capability, as a result, the fluid velocity enhances. Figure 3 signifies that the axial velocity $f'(\eta)$ reduces with the flourishing Darcy effect. Figure 4 manifested that the fluid velocity lessens with the rising effect of the magnetic field, because the resistive force, which is generated due to magnetic force contests the fluid flow. The fluid velocity declines under the consequences of parameter n as shown in Fig. 5.

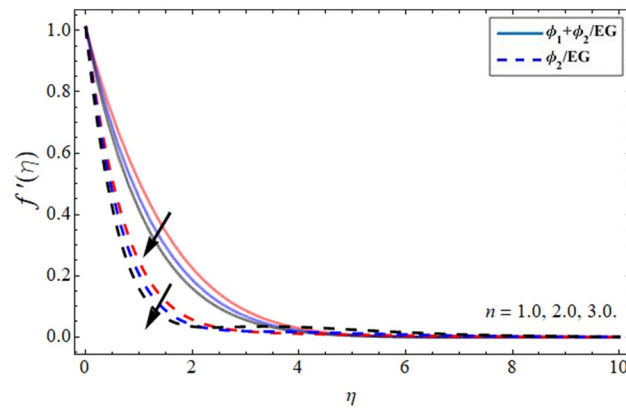


Figure 5. Velocity $f'(\eta)$ outlines versus the effect of parameter n .

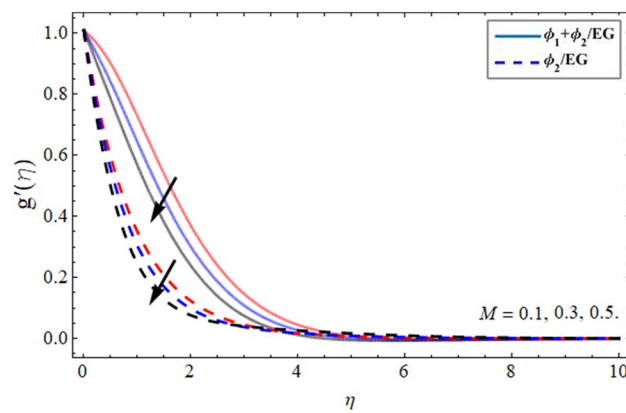


Figure 6. Velocity $g'(\eta)$ outlines versus the effect of magnetic term M .

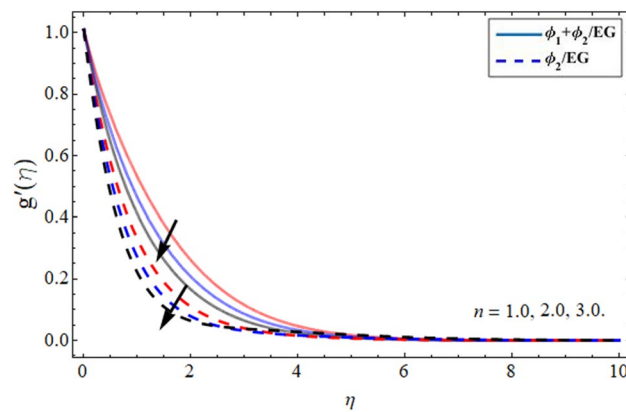


Figure 7. Velocity $g'(\eta)$ outlines versus the effect of parameter n .

Figures 6 and 7 illustrated that the velocity field in radial direction $g'(\eta)$ diminishes with the growing values of magnetic effect and parameter n respectively. The Lorentz force formed due to magnetic term variation opposes the flow field, which costs in the lessening of the radial velocity field. Similarly, the increment of parameter n also reduces the momentum boundary layer as presented in Fig. 7.

Figures 8, 9, 10 and 11 revealed the presentation of energy contour against the flourishing trend of nanoparticle volume fraction ϕ , parameter n , versus thermal Deborah number λ_E and heat generation term h_s respectively. Figure 8 elaborated that the variation of nanomaterials in the base fluid significantly magnifies its thermal conduction, which is more effective for industrial uses. The thermal conductivity of nanoparticles is

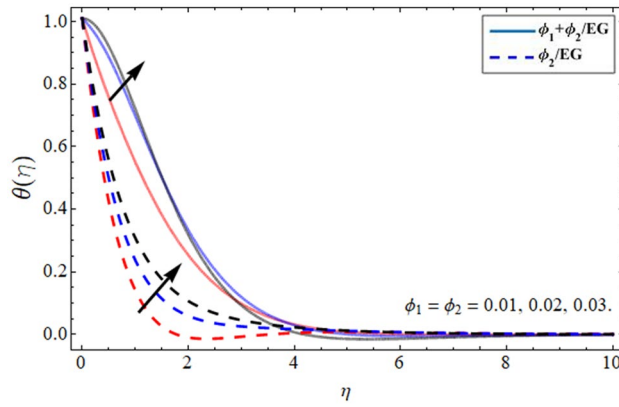


Figure 8. Energy $\theta(\eta)$ outlines versus the effect of nanoparticle volume friction ϕ .

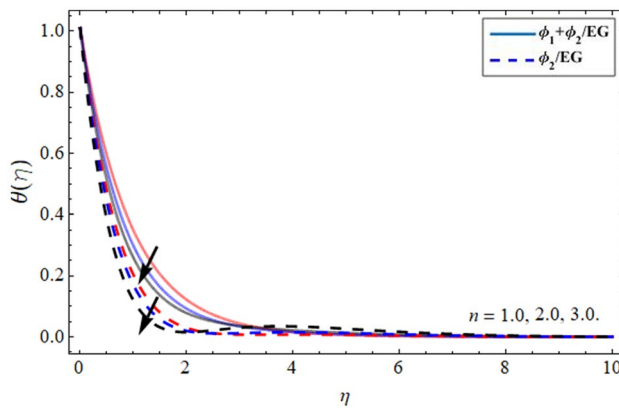


Figure 9. Energy $\theta(\eta)$ outlines versus the effect of parameter n .

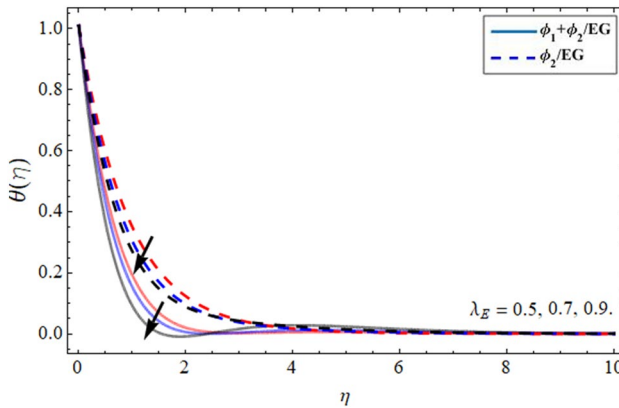


Figure 10. Energy $\theta(\eta)$ outlines versus the effect of thermal Deborah number λ_E .

greater than the ethylene glycol, that's why its addition boosts the thermal property of the carrier fluid. Figure 9 demonstrated that the energy profile declines with the upshot of parameter n . Figure 10 and 11 display that the thermal energy outline decreases with the upshot of thermal Deborah number λ_E while enhancing with the variation of heat source term hs . The heat source term augments the internal energy of the fluid, which encourages the fluid energy profile to enhance.

Table 1 reported the experimental values of nanoparticulate ($\phi_1 = \phi_C$, $\phi_2 = \phi_{Cu}$) and base fluid (ethylene glycol). Table 2 show the comparative analysis between nanofluid and hybrid nanofluid for skin friction along x ($-(\text{Re})^{-\frac{1}{2}} C_f$) and y ($-(\text{Re})^{-\frac{1}{2}} C_g$) direction and Nusselt number ($-(\text{Re})^{-\frac{1}{2}} C_{Nu}$). It revealed that the energy

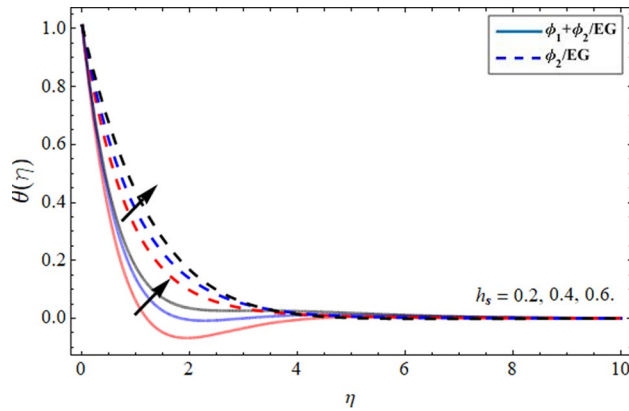


Figure 11. Energy $\theta(\eta)$ outlines versus the effect of heat generation term h_s .

	ρ (kg/m ³)	C_p (j/kgK)	k (W/mK)	σ (S/m)
Ethylene glycol	1114	2415	0.252	5.5×10^{-6}
Copper ($\phi_2 = \phi_{Cu}$)	8933	385	401	5.96×10^7
Graphene $\phi_1 = \phi_C$	2250	2100	2500	1.0×10^7

Table 1. The experimental values of base fluid (ethylene glycol) and nano particulates (copper and graphene⁵⁸).

	Nanofluid			Hybrid Nanofluid		
	$-(Re)^{-\frac{1}{2}} C_f$	$-(Re)^{-\frac{1}{2}} C_g$	$-(Re)^{-\frac{1}{2}} C_{Nu}$	$-(Re)^{-\frac{1}{2}} C_f$	$-(Re)^{-\frac{1}{2}} C_g$	$-(Re)^{-\frac{1}{2}} C_{Nu}$
N						
1.0	0.053003848	0.227327334	0.077382179	1.190488671	1.694350204	2.30917111
2.0	0.199883781	0.371279545	0.778005638	1.269149144	1.695060775	2.30830922
3.0	0.245493938	0.388009192	1.097857874	1.368321032	1.713010775	2.64498558
M						
0.0	0.344535715	0.447423914	1.334285223	0.292111797	0.358230717	1.42199998
0.2	0.427622087	0.516102601	1.267066226	0.178750768	0.138358081	1.33935047
0.4	0.606583762	0.680803897	1.101385769	0.062545122	0.015291717	1.25861093
lambda_E						
0.0	0.727414454	0.686095548	0.389867706	0.416526708	0.679956092	5.07556644
0.6	0.857743852	0.719203214	1.353232227	0.526997918	0.731764147	5.09927908
1.1	0.886982272	0.751114887	1.314949813	0.580192798	0.802449387	4.17826838
h_s						
0.0	0.327677637	0.372891414	2.026693234	0.269941338	0.467279475	7.06024758
0.3	0.327677637	0.372891414	1.165464671	0.269941338	0.467279475	6.01929661
0.7	0.427677636	0.472891413	2.189427429	0.369941337	0.567279474	6.16243263

Table 2. Statistical outcomes for physical quantities, such as skin friction $\left(- (Re)^{-\frac{1}{2}} C_f, -(Re)^{-\frac{1}{2}} C_g\right)$ and Nusselt number $\left(- (Re)^{-\frac{1}{2}} C_{Nu}\right)$ in case of both nanofluid and hybrid nanofluid.

conduction of hybrid nanofluid as compared to nanofluid is greater. The heat source and thermal Deborah number enhance the skin friction and Nusselt number remarkably. Table 3 shows the comparative evaluation of the published results with the current outcomes for skin friction and Nusselt number. It can be seen that the present results show closed adjustment with the existing literature, which ensure the validity of the results and proposed technique.

Parameters	$-(Re)^{-\frac{1}{2}} C_f$	$-(Re)^{-\frac{1}{2}} C_f$	$-(Re)^{-\frac{1}{2}} C_{Nu}$	$-(Re)^{-\frac{1}{2}} C_{Nu}$
<i>M</i>	Sadiq ⁵⁹	Present results	Sadiq ⁵⁹	Present results
0.0	0.4445357154	0.4445357455	2.434285223	2.434285423
0.3	0.5276220806	0.5276220932	2.367066226	2.367066441
0.7	0.7065837651	0.7065837753	2.201385769	2.201385873
<i>n</i>				
1.0	0.1530038477	0.153003868	0.0773821732	0.0773821753
2.0	0.2998837840	0.2998837952	1.878005638	1.878005852
3.0	0.3454939329	0.3454939651	2.197857874	2.197857976

Table 3. Comparative assessment of published results with the current outcomes.

Conclusion

The three-dimensional Darcy Forchheimer hybrid nanofluid flow has been studied under the impact of heat generation and magnetic field over a two-dimensionally stretchable moving permeable surface. The phenomena are characterized as a nonlinear system of PDEs. The solution has been obtained through the PCM procedure. The key findings are:

- The accumulation of copper and graphene nanoparticulate to the base fluid ethylene glycol significantly improves velocity and heat conduction rate over a stretching surface.
- The axial velocity contour boosts with the addition of hybrid NPs in EG while reducing with the flourishing Darcy and magnetic effect.
- The variation of magnetic effect and parameter *n* diminishes the velocity field towards the radial direction $g'(\eta)$.
- The thermal energy profile decreases with the effect of thermal Deborah number and parameter *n*. while enhancing with the variation of heat source term.
- As compared to the nanofluid (copper or graphene), hybrid nanofluid (copper + graphene) has a greater tendency for thermal energy conduction.
- The rising influence of heat source enhances the skin friction, while declines the Nusselt number.
- The effect of magnetic force also boosts the skin friction, while declines the Nusselt number.

Data availability

The data that supports the findings of this study are available within the article.

Received: 23 March 2022; Accepted: 10 June 2022

Published online: 21 June 2022

References

1. Ullah, I. Heat transfer enhancement in Marangoni convection and nonlinear radiative flow of gasoline oil conveying Boehmite alumina and aluminum alloy nanoparticles. *Int. Commun. Heat Mass Transf.* **132**, 105920 (2022).
2. Ullah, I. Activation energy with exothermic/endothemic reaction and Coriolis force effects on magnetized nanomaterials flow through Darcy–Forchheimer porous space with variable features. *Waves Random Complex Med.* 1–14 (2022).
3. Algehyne, E. A., Alhusayni, Y. Y., Tassaddiq, A., Saeed, A., & Bilal, M. The study of nanofluid flow with motile microorganism and thermal slip condition across a vertical permeable surface. *Waves Random and Complex Med.* 1–18 (2022).
4. Ullah, Z., Ullah, I., Zaman, G. & Sun, T. C. A numerical approach to interpret melting and activation energy phenomenon on the magnetized transient flow of Prandtl–Eyring fluid with the application of Cattaneo–Christov theory. *Waves Random Complex Med.* 1–21 (2022).
5. Machireddy, G. R. & Naramgari, S. Heat and mass transfer in radiative MHD Carreau fluid with cross diffusion. *Ain Shams Eng. J.* **9**(4), 1189–1204 (2018).
6. Bilal, M. *et al.* Parametric simulation of micropolar fluid with thermal radiation across a porous stretching surface. *Sci. Rep.* **12**(1), 1–11 (2022).
7. Minakov, A. V., Rudyak, V. Y. & Pryazhnikov, M. I. Rheological behavior of water and ethylene glycol based nanofluids containing oxide nanoparticles. *Colloids Surf., A* **554**, 279–285 (2018).
8. Al-Mubaddel, F. S., Allehiyani, F. M., Nofal, T. A., Alam, M. M., Ali, A., & Asamoah, J. K. K. Rheological model for generalized energy and mass transfer through hybrid nanofluid flow comprised of magnetized cobalt ferrite nanoparticles. *J. Nanomater.*
9. Cheng, C. Y. Combined heat and mass transfer in natural convection flow from a vertical wavy surface in a power-law fluid saturated porous medium with thermal and mass stratification. *Int. Commun. Heat Mass Transf.* **36**(4), 351–356 (2009).
10. Javid Sarafan, M., Alizadeh, R., Fattahi, A., Valizadeh Ardalani, M. & Karimi, N. Heat and mass transfer and thermodynamic analysis of power-law fluid flow in a porous microchannel. *J. Therm. Anal. Calorim.* **141**(5), 2145–2164 (2020).
11. Chavaraddi, K. B., Chandaragi, P. L., Gouder, P. M., & Marali, G. B. Influence of Electric and Magnetic Fields on Rayleigh–Taylor Instability in a Power-Law Fluid. In *Mathematical Modeling, Computational Intelligence Techniques and Renewable Energy* (pp. 241–253). Springer, Singapore, (2022)
12. Alsallami, S. A. M., Zahir, H., Muhammad, T., Hayat, A. U., Riaz Khan, M. & Ali A. “Numerical simulation of Marangoni Maxwell nanofluid flow with Arrhenius activation energy and entropy anatomization over a rotating disk. *Waves Random Complex Med.* 1–19 (2022)
13. Arefmanesh, A., Arani, M. M. & Arani, A. A. A. Dynamics of a bubble in a power-law fluid confined within an elastic solid. *Eur. J. Mech.-B/Fluids* **94**, 29–36 (2022).

14. Bilal, M., Ayed, H., Saeed, A., Brahmia, A., Gul, T., & Kumam, P. The parametric computation of nonlinear convection magneto-hydrodynamic nanofluid flow with internal heating across a fixed and spinning disk. *Waves Random Complex Med.*, 1–16 (2022)
15. Elattar, S. *et al.* Computational assessment of hybrid nanofluid flow with the influence of hall current and chemical reaction over a slender stretching surface. *Alex. Eng. J.* **61**(12), 10319–10331 (2022).
16. Naveen Kumar, R., Gowda, R. J., Giresha, B. J. & Prasannakumara, B. C. Non-Newtonian hybrid nanofluid flow over vertically upward/downward moving rotating disk in a Darcy-Forchheimer porous medium. *Eur. Phys. J. Special Top.* **230**(5), 1227–1237 (2021).
17. Sarada, K., Gowda, R. J. P., Sarris, I. E., Kumar, R. N. & Prasannakumara, B. C. Effect of magnetohydrodynamics on heat transfer behaviour of a non-Newtonian fluid flow over a stretching sheet under local thermal non-equilibrium condition. *Fluids* **6**(8), 264 (2021).
18. Punith Gowda, R. J., Naveen Kumar, R., Jyothi, A. M., Prasannakumara, B. C. & Sarris, I. E. Impact of binary chemical reaction and activation energy on heat and mass transfer of marangoni driven boundary layer flow of a non-Newtonian nanofluid. *Processes* **9**(4), 702 (2021).
19. Gowda, R. P. *et al.* Computational modelling of nanofluid flow over a curved stretching sheet using Koo-Kleinstreuer and Li (KKL) correlation and modified Fourier heat flux model. *Chaos, Solitons Fract.* **145**, 110774 (2021).
20. Punith Gowda, R. J., Naveen Kumar, R., Jyothi, A. M., Prasannakumara, B. C. & Nisar, K. S. KKL correlation for simulation of nanofluid flow over a stretching sheet considering magnetic dipole and chemical reaction. *ZAMM-J. Appl. Math. Mech./Zeitschrift für Angewandte Mathematik und Mechanik* **101**(11), e202000372 (2021).
21. Varun Kumar, R. S., Alhadhrami, A., Punith Gowda, R. J., Naveen Kumar, R. & Prasannakumara, B. C. Exploration of Arrhenius activation energy on hybrid nanofluid flow over a curved stretchable surface. *ZAMM-J. Appl. Math. Mech./Zeitschrift für Angewandte Mathematik und Mechanik* **101**(12), e202100035 (2021).
22. Gowda, R. P., Naveenkumar, R., Madhukesh, J. K., Prasannakumara, B. C. & Gorla, R. S. R. Theoretical analysis of SWCNT-MWCNT/H₂O hybrid flow over an upward/downward moving rotating disk. *Proc. Inst. Mech. Eng., Part N: J. Nanomater., Nanoeng. Nanosyst.* **235**(3–4), 97–106 (2021).
23. Punith Gowda, R. J., Naveen Kumar, R. & Prasannakumara, B. C. Two-phase Darcy-Forchheimer flow of dusty hybrid nanofluid with viscous dissipation over a cylinder. *Int. J. Appl. Comput. Math.* **7**(3), 1–18 (2021).
24. Nazeer, M. *et al.* Theoretical study of MHD electro-osmotically flow of third-grade fluid in micro channel. *Appl. Math. Comput.* **420**, 126868 (2022).
25. Ma, T., Guo, Z., Lin, M. & Wang, Q. Recent trends on nanofluid heat transfer machine learning research applied to renewable energy. *Renew. Sustain. Energy Rev.* **138**, 110494 (2021).
26. Kumar, R. N. *et al.* Impact of magnetic dipole on ferromagnetic hybrid nanofluid flow over a stretching cylinder. *Phys. Scr.* **96**(4), 045215 (2021).
27. Khan, M. I. *et al.* Marangoni convective flow of hybrid nanofluid (MnZnFe₂O₄-NiZnFe₂O₄-H₂O) with darcy forchheimer medium. *Ain Shams Eng. J.* **12**(4), 3931–3938 (2021).
28. Chu, Y. M. *et al.* Combined impact of Cattaneo-Christov double diffusion and radiative heat flux on bio-convective flow of Maxwell liquid configured by a stretched nano-material surface. *Appl. Math. Comput.* **419**, 126883 (2022).
29. Zhao, T. H., Ijaz Khan, M., Chu, Y.-M. Artificial neural networking (ANN) analysis for heat and entropy generation in flow of non-Newtonian fluid between two rotating disks, *Math. Methods Appl. Sci.*, 2021.
30. Zhao, T. H., Wang, M. K., Zhang, W. & Chu, Y. M. Quadratic transformation inequalities for Gaussian hypergeometric function. *J. Inequal. Appl.* **2018**(1), 1–15 (2018).
31. Jia, L. *et al.* Ultrasound-enhanced precision tumor theranostics using cell membrane-coated and pH-responsive nanoclusters assembled from ultrasmall iron oxide nanoparticles. *Nano Today* **36**, 101022 (2021).
32. Schwaminger, S. P., Schwarzenberger, K., Gatzemeier, J., Lei, Z. & Eckert, K. Magnetically induced aggregation of iron oxide nanoparticles for carrier flotation strategies. *ACS Appl. Mater. Interfaces.* **13**(17), 20830–20844 (2021).
33. Lv, Y. P. *et al.* Numerical approach towards gyrotactic microorganisms hybrid nanoliquid flow with the hall current and magnetic field over a spinning disk. *Sci. Rep.* **11**(1), 1–13 (2021).
34. Chu, Y. M., Bashir, S., Ramzan, M., & Malik, M. Y. Model-based comparative study of magnetohydrodynamics unsteady hybrid nanofluid flow between two infinite parallel plates with particle shape effects. *Math. Methods Appl. Sci.* (2022)
35. Chu, Y. M., Nazir, U., Sohail, M., Selim, M. M. & Lee, J. R. Enhancement in thermal energy and solute particles using hybrid nanoparticles by engaging activation energy and chemical reaction over a parabolic surface via finite element approach. *Fract. Fract.* **5**(3), 119 (2021).
36. Jin, F., Qian, Z.-S., Chu, Y.-M. & ur Rahman, M. On nonlinear evolution model for drinking behavior under Caputo-Fabrizio derivative. *J. Appl. Anal. Comput.* **12**(2), 790–806. <https://doi.org/10.11948/20210357> (2022).
37. Tassaddiq, A. *et al.* Heat and mass transfer together with hybrid nanofluid flow over a rotating disk. *AIP Adv.* **10**(5), 055317 (2020).
38. Bilal, M., Gul, T., Alsubie, A. & Ali, I. Axisymmetric hybrid nanofluid flow with heat and mass transfer amongst the two gyrating plates. *ZAMM-J. Appl. Math. Mech./Zeitschrift für Angewandte Mathematik und Mechanik* **101**(11), e202000146 (2021).
39. Ullah, I., Hayat, T., Aziz, A. & Alsaedi, A. Significance of entropy generation and the coriolis force on the three-dimensional non-darcy flow of ethylene-glycol conveying carbon nanotubes (SWCNTs and MWCNTs). *J. Non-Equilib. Thermodyn.* **47**(1), 61–75 (2022).
40. Alharbi, K. A. M. *et al.* Computational valuation of darcy ternary-hybrid nanofluid flow across an extending cylinder with induction Effects. *Micromachines* **13**(4), 588 (2022).
41. Ullah, I., Hayat, T. & Alsaedi, A. Optimization of entropy production in flow of hybrid nanomaterials through Darcy–Forchheimer porous space. *J. Therm. Anal. Calorim.*, 1–10 (2021)
42. Zhang, X. H. *et al.* The parametric study of hybrid nanofluid flow with heat transition characteristics over a fluctuating spinning disk. *PLoS ONE* **16**(8), e0254457 (2021).
43. Kumar, R. N. *et al.* Inspection of convective heat transfer and KKL correlation for simulation of nanofluid flow over a curved stretching sheet. *Int. Commun. Heat Mass Transf.* **126**, 105445 (2021).
44. Shuaib, M., Bilal, M. & Qaisar, S. Numerical study of hydrodynamic molecular nanoliquid flow with heat and mass transmission between two spinning parallel plates. *Phys. Scr.* **96**(2), 025201 (2020).
45. Li, Y. X. *et al.* Dynamics of aluminum oxide and copper hybrid nanofluid in nonlinear mixed Marangoni convective flow with entropy generation: Applications to renewable energy. *Chin. J. Phys.* **73**, 275–287 (2021).
46. Xiong, P. Y. *et al.* Comparative analysis of (Zinc ferrite, Nickel Zinc ferrite) hybrid nanofluids slip flow with entropy generation. *Mod. Phys. Lett. B* **35**(20), 2150342 (2021).
47. Zhao, T. H., Wang, M. K. & Chu, Y. M. Concavity and bounds involving generalized elliptic integral of the first kind. *J. Math. Inequal.* **15**(2), 701–724 (2021).
48. Christov, C. I. On frame indifferent formulation of the Maxwell-Cattaneo model of finite-speed heat conduction. *Mech. Res. Commun.* **36**(4), 481–486 (2009).
49. Sui, J., Zheng, L. & Zhang, X. Boundary layer heat and mass transfer with Cattaneo-Christov double-diffusion in upper-convected Maxwell nanofluid past a stretching sheet with slip velocity. *Int. J. Therm. Sci.* **104**, 461–468 (2016).
50. Hafeez, A., Khan, M. & Ahmed, J. Flow of oldroyd-b fluid over a rotating disk with Cattaneo-Christov theory for heat and mass fluxes. *Comput. Methods Progr. Biomed.* **191**, 105374 (2020).

51. Manjunatha, P. T. *et al.* Significance of stefan blowing and convective heat transfer in nanofluid flow over a curved stretching sheet with chemical reaction. *J. Nanofluids* **10**(2), 285–291 (2021).
52. Naveen Kumar, R., Suresha, S., Gowda, R. J., Megalamani, S. B. & Prasannakumara, B. C. Exploring the impact of magnetic dipole on the radiative nanofluid flow over a stretching sheet by means of KKL model. *Pramana* **95**(4), 1–9 (2021).
53. Madhukesh, J. K., Alhadhrani, A., Naveen Kumar, R., Punith Gowda, R. J., Prasannakumara, B. C., & Varun Kumar, R. S. Physical insights into the heat and mass transfer in Casson hybrid nanofluid flow induced by a Riga plate with thermophoretic particle deposition. *Proc. Inst. Mech. Eng., Part E: J. Process Mech. Eng.*, 09544089211039305. (2021)
54. Madhukesh, J. K. *et al.* Numerical simulation of AA7072-AA7075/water-based hybrid nanofluid flow over a curved stretching sheet with Newtonian heating: A non-Fourier heat flux model approach. *J. Mol. Liq.* **335**, 116103 (2021).
55. Algehyne, E. A. *et al.* Numerical simulation of bioconvective Darcy Forchhemier nanofluid flow with energy transition over a permeable vertical plate. *Sci. Rep.* **12**(1), 1–12 (2022).
56. Zhuang, Y. J., Yu, H. Z. & Zhu, Q. Y. A thermal non-equilibrium model for 3D double diffusive convection of power-law fluids with chemical reaction in the porous medium. *Int. J. Heat Mass Transf.* **115**, 670–694 (2017).
57. Gowda, R. J., Kumar, R. N., Rauf, A., Prasannakumara, B. C., & Shehzad, S. A. Magnetized flow of sutterby nanofluid through cattaneo-christov theory of heat diffusion and stefan blowing condition. *Appl. Nanosci.*, 1–10 (2021)
58. Bhattacharyya, A., Sharma, R., Hussain, S. M., Chamkha, A. J., & Mamatha, E. A numerical and statistical approach to capture the flow characteristics of Maxwell hybrid nanofluid containing copper and graphene nanoparticles. *Chin. J. Phys.* (2021)
59. Sadiq, M. A. Non fourier heat transfer enhancement in power law fluid with mono and hybrid nanoparticles. *Sci. Rep.* **11**(1), 1–14 (2021).
60. Shuaib, M., Shah, R. A., Durrani, I. & Bilal, M. Electrokinetic viscous rotating disk flow of Poisson-Nernst-Planck equation for ion transport. *J. Mol. Liq.* **313**, 113412 (2020).
61. Shuaib, M., Shah, R. A. & Bilal, M. Von-Karman rotating flow in variable magnetic field with variable physical properties. *Adv. Mech. Eng.* **13**(2), 1687814021990463 (2021).
62. Wang, F. *et al.* Numerical solution of traveling waves in chemical kinetics: time-fractional fishers equations. *Fractals* **30**(02), 2240051 (2022).
63. Zhao, T. H., Chu, H. H. & Chu, Y. M. Optimal Lehmer mean bounds for the nth power-type toader means OF $n=1, 2, 3$. *J. Math. Inequal.* **16**(1), 157–159 (2022).

Acknowledgements

The authors extend their appreciation to the Deanship of Scientific Research at King Khalid University for funding this work through Large Groups “(Project under grant number (RGP.2/116/43))”.

Author contributions

M.B. wrote the original manuscript and performed the numerical simulation. A.A. and A.A., reviewed the mathematical results and restructured the manuscript. Also A.A., and M.A. responses the reviewer’s queries. H.H. and M.A. do the data curation, conceptualization and reviewed the manuscript. The validation, funding acquisitions and supervision belongs to K.M. All authors are agreed on the final draft of the submission file.

Funding

This research was supported by the fundamental fund of Khon Kaen University. “The research on Non-Fourier energy transmission in Power-law hybrid nanofluid flow over a moving sheet by Khon Kaen University, Department of Mathematics, Faculty of Science, has received funding support from the National Science, Research and Innovation Fund.” or “NSRF”.

Competing interests

The authors declare no competing interests.

Additional information

Correspondence and requests for materials should be addressed to K.M.

Reprints and permissions information is available at www.nature.com/reprints.

Publisher’s note Springer Nature remains neutral with regard to jurisdictional claims in published maps and institutional affiliations.



Open Access This article is licensed under a Creative Commons Attribution 4.0 International License, which permits use, sharing, adaptation, distribution and reproduction in any medium or format, as long as you give appropriate credit to the original author(s) and the source, provide a link to the Creative Commons licence, and indicate if changes were made. The images or other third party material in this article are included in the article’s Creative Commons licence, unless indicated otherwise in a credit line to the material. If material is not included in the article’s Creative Commons licence and your intended use is not permitted by statutory regulation or exceeds the permitted use, you will need to obtain permission directly from the copyright holder. To view a copy of this licence, visit <http://creativecommons.org/licenses/by/4.0/>.

© The Author(s) 2022